Gan, Tian; Ding, Guochang; Chen, Boran; Zhi, Xiaojing; Li, Ping; Yao, Xueli; Hou, Nianjun; Fan, Lijun; Zhao, Yicheng; Li, Yongdan

Effects of manganese oxides on the activity and stability of Ni-$Ce_{0.8}Sm_{0.2}O_{1.9}$ anode for solid oxide fuel cells with methanol as the fuel

Published in:
Catalysis Today

DOI:
10.1016/j.cattod.2018.01.014

Published: 15/06/2019

Document Version
Peer-reviewed accepted author manuscript, also known as Final accepted manuscript or Post-print

Please cite the original version:
Gan, T., Ding, G., Chen, B., Zhi, X., Li, P., Yao, X., Hou, N., Fan, L., Zhao, Y., & Li, Y. (2019). Effects of manganese oxides on the activity and stability of Ni-$Ce_{0.8}Sm_{0.2}O_{1.9}$ anode for solid oxide fuel cells with methanol as the fuel. *Catalysis Today*, *330*, 222-227. https://doi.org/10.1016/j.cattod.2018.01.014

Effects of manganese oxides on the activity and stability of Ni-$Ce_{0.8}Sm_{0.2}O_{1.9}$ anode for solid oxide fuel cells with methanol as the fuel

Tian Gan[1,2], Guochang Ding[1,2], Boran Chen[1,2], Xiaojing Zhi[1,2], Ping Li[1,2], Xueli Yao[1,2], Nianjun Hou[1,2], Lijun Fan[1,2], Yicheng Zhao[1,2*], Yongdan Li[1,2,3*]

[1]State Key Laboratory of Chemical Engineering (Tianjin University), Tianjin Key Laboratory of Applied Catalysis Science and Technology, School of Chemical Engineering, Tianjin University, Tianjin 300072, China

[2]Collaborative Innovation Center of Chemical Science and Engineering (Tianjin), Tianjin, 300072, China.

[3]Department of Chemical and Metallurgical Engineering, School of Chemical Engineering, Aalto University, Kemistintie 1, Espoo, P.O. Box 16100, FI-00076 Aalto Finland

Abstract

Ni-MnO_x-$Ce_{0.8}Sm_{0.2}O_{1.9}$ (SDC) composites are synthesized and investigated as anode materials of solid oxide fuel cells fed with methanol. The lowest anodic polarization resistance is obtained when the molar ratio of Mn to Ni is 0.05:0.95. The high catalytic activity is attributed to the transfer of electrons from Ni to Mn and the increase of the content of the lattice oxygen in the anode. The single cell with that anode and SDC-carbonate composite electrolyte exhibits a maximum power density of 722 mW cm^{-2} at 700 °C. Mn also increases the resistance to carbon deposition of the anode due to the high lattice oxygen content and the redox cycle of the Mn species. The stability of the single cell is enhanced with the increase of the content of Mn in the anode.

---

*Corresponding author. Email: zhaoyicheng@tju.edu.cn; Tel: +86-22-27405613; Fax: +86-22-27405243 (Y. Zhao)

*Corresponding author. Email: ydli@tju.edu.cn; Tel: +86-22-27405613; Fax: +86-22-27405243 (Y. Li)

Keywords: Solid oxide fuel cell; Anode; Methanol electro-oxidation; Carbon deposition; Manganese oxides; Lattice oxygen

1. Introduction

Solid oxide fuel cells (SOFCs) are one of the most promising devices for the direct conversion of chemical energy in fuels into electric power [1] . SOFCs exhibit many advantages such as high energy conversion efficiency, low emissions and high fuel flexibility. The high operating temperature (700-1000 °C) of SOFCs accelerates the anodic reactions, which allows the substitution of pure H_2 by other readily available fuels, such as hydrocarbons, syngas, ammonia and even solid carbon [2-6]. Among hydrocarbons, methanol (CH_3OH), a renewable resource that could be obtained from biomass fermentation, possesses a high volumetric energy density and low impurity content, making it a potential fuel for SOFCs [7-10].

The Ni-based cermet has been considered as the most promising anode material for SOFCs fed with H_2 due to its high catalytic activity, sufficient electrical conductivity and low cost [11]. However, with hydrocarbons as the fuel, the high catalytic activity of Ni towards the formation of C-C bonds leads to serious carbon deposition on the anode and rapid degradation of the cell [3, 12]. It has been proved that the partial substitution of Ni by some other metals is an effective approach to alleviate carbon deposition and improve the stability of the fuel cell. Kan *et al.* [13] reported that the doping of Sn in Ni-yttria stabilized zirconia (Ni-YSZ) anode significantly improved the long-term stability of the single cell with humidified methane as the fuel, which exhibited a stable output power density of 0.41 W cm^{-2} at 650 °C for 37 h. Cheng *et al.* [14] added Cu into Ni-$Ce_{0.8}Sm_{0.2}O_{1.9}$ (SDC) anode. The amount of carbon nucleation sites is decreased by the formation of Ni-Cu alloy, and the carbon deposition on the anode in a dry methane atmosphere is suppressed significantly. It is worth noting that

SDC itself also inhibits carbon deposition attributed to its high oxygen ionic conductivity [15]. Qu et al. [6] added basic oxide additives, such as SrO, BaO and La_2O_3, in the Ni-SDC anode. These basic oxides efficiently prevented Ni agglomeration and enhanced the coking resistance, resulting in a high stability of the cell with methane as fuel.

Recently, Chen *et al.* [16] found that the Mn–Ce–O composite catalyst shows a superior catalytic activity for the wet oxidation of phenol. The increase of catalytic active sites was ascribed to the higher oxidation state of manganese oxide species and the electron-rich surface which can efficiently activate adsorbed oxygen. Meanwhile, the interaction between Mn and Ce significantly enhanced the oxygen mobility and oxygen storage capacity of manganese and cerium oxides on the surface of catalyst, facilitating the removal of carbonaceous deposits. Seok *et al.* [17] reported that MnO-promoted Ni-Al_2O_3 catalyst showed an improved stability for CO_2 reforming of methane. The partial blockage of surface nickel sites by MnO and the moderate basicity of manganese oxides result in a higher resistance to carbon deposition. Zhao *et al.* [18] found that the polarization resistance of Ni-SDC anode with dry CH_4 as the fuel is significantly reduced by the modification with MnO-Co composite, while its stability declines simultaneously due to the severer carbon deposition. In this work, Ni-MnO_x-SDC composite is synthesized and studied as the anode material of SOFCs with methanol as the fuel for the first time. The effects of MnO_x on the catalytic activity and stability of the anode are examined and discussed.

2. Experimental

2.1. Material preparation

NiO-yMnO_x-SDC ($0 \leq y \leq 0.2$) powders were synthesized with a hydrothermal technique [19]. The mole ration of the total amount of Ni and Mn to SDC was 7:3. Stoichiometric $Ce(NO_3)_3·6H_2O$ (99.5%, Guangfu fine chemical, Ltd., China), $Sm(NO_3)_3·6H_2O$ (99.9%, Guangfu fine chemical, Ltd., China), $Ni(NO_3)_2·6H_2O$ (98%, Beijing HWRK Chem Co., Ltd., China) and $Mn(NO_3)_2·6H_2O$ (AR, 50 wt.% in H_2O, Aladdin) were dissolved in deionized water with a total metal ion concentration of 0.15 mol L^{-1} and then heated at 70 °C with constant stir. After complete dissolution of the metal nitrates, urea (Guangfu fine chemical, Ltd., China) was added into the solution with a concentration of 1 mol L^{-1}. The solution was transferred into a hydrothermal reactor and kept at 140 °C for 5 h. The precipitation obtained was washed with deionized water for 3 times, dried at 100 °C for 4 h, and then calcined in air at 700 °C for 2 h. The molar ratios of Mn to Ni in the anodes were 0:1, 0.03: 0.97, 0.05: 0.95, 0.1: 0.9 and 0.2: 0.8, which were marked as NiO-SDC, NiO-3MnO_x-SDC, NiO-5MnO_x-SDC, NiO-10MnO_x-SDC and NiO-20MnO_x-SDC, respectively. The powders were reduced in H_2 at 700 °C for 2 h for the following characterization.

The electrolyte was a composite of SDC and $(Li_{0.67}Na_{0.33})_2CO_3$ with a weight ratio of 7:3. The SDC was prepared through a similar hydrothermal approach. The cathode was composed of 30 wt.% composite electrolyte and 70 wt.% lithiated NiO. Detailed preparation processes of the electrolyte and cathode materials were described in previous works [20, 21].

2.2. Characterization

The X-ray diffraction (XRD) patterns of the anode powders before and after reduction were recorded using a D8 Focus diffractometer (Bruker Corp., Germany) with Cu-Kα radiation, 40 kV and 200 mA, at a scanning rate of 8° min^{-1}. Hydrogen temperature-programmed reduction (H_2-TPR) was carried out in a quartz tube reactor. About 100 mg of the catalyst sample (140-160 mesh) was pretreated in Ar (>99.999%, 30 mL min^{-1}, STP) at 200 °C for 1 h. After a natural cooling procedure, the test was performed with 5% H_2-95% Ar (50 mL min^{-1}, STP) as the reductant from room temperature to 800 °C at a heating rate of 10 °C min^{-1}. To study the surface property of the reduced samples, the X-ray photoelectron spectroscopy (XPS) was recorded using a XLESCALAB 250Xi electron spectrometer (VG Scientific) with Al-Kα radiation.

The reduced anode powder was treated in gasified anhydrous methanol (150 mL min^{-1}, STP) at 700 °C for 4 h. After the sample cooled down to room temperature in Ar atmosphere, the mass of the deposited carbon was measured with a PerkinElmer Diamond Thermogravimetric analyzer (TGA) from room temperature to 900 °C at a heating rate of 10 °C min^{-1} in air.

2.3. Fuel cell test

The fabricating process of the single cell has been described in previous works [22]. Briefly, the electrolyte and cathode layers of the cell were co-pressed at 500 MPa and subsequently sintered at 700 °C in air for 1 h. The thicknesses of the electrolyte and cathode layers were 0.65 and 0.35 mm, respectively [23, 24]. The anode powder was made into slurry with a binder (V006, Heraeus Ltd.), and then screen-printed on the electrolyte layer, followed by sintering at 700 °C in air for 1 h. Ag paste as current collector was coated on both sides of the cell. The geometric surface area of the electrodes was 0.64 cm^2. The surface and cross-sectional morphology of the cell was characterized with a scanning electron microscope (SEM, Hitachi, S-4800) equipped with an energy dispersive X-ray spectrometer (EDX).

Before the cell test, the anode was reduced in H_2 for 2 h at 700 °C. Then the *I-V* curves of the cell were recorded with an electrochemical workstation (VersaSTAT 3, Ametek) in the range of 500-700 °C with gasified anhydrous methanol (100 ml min^{-1}, STP) and O_2 (30 ml min^{-1}, STP) as the fuel and oxidant, respectively. The electrochemical impedance spectroscopy (EIS) of the cell was recorded under the open circuit condition in the frequency range from 1M to 0.1 Hz with an amplitude of 10 mV. The stability of the cells was tested at 700 ºC under a constant current density of 200 mA cm^{-2}.

3. Results and discussion

3.1. Characterization

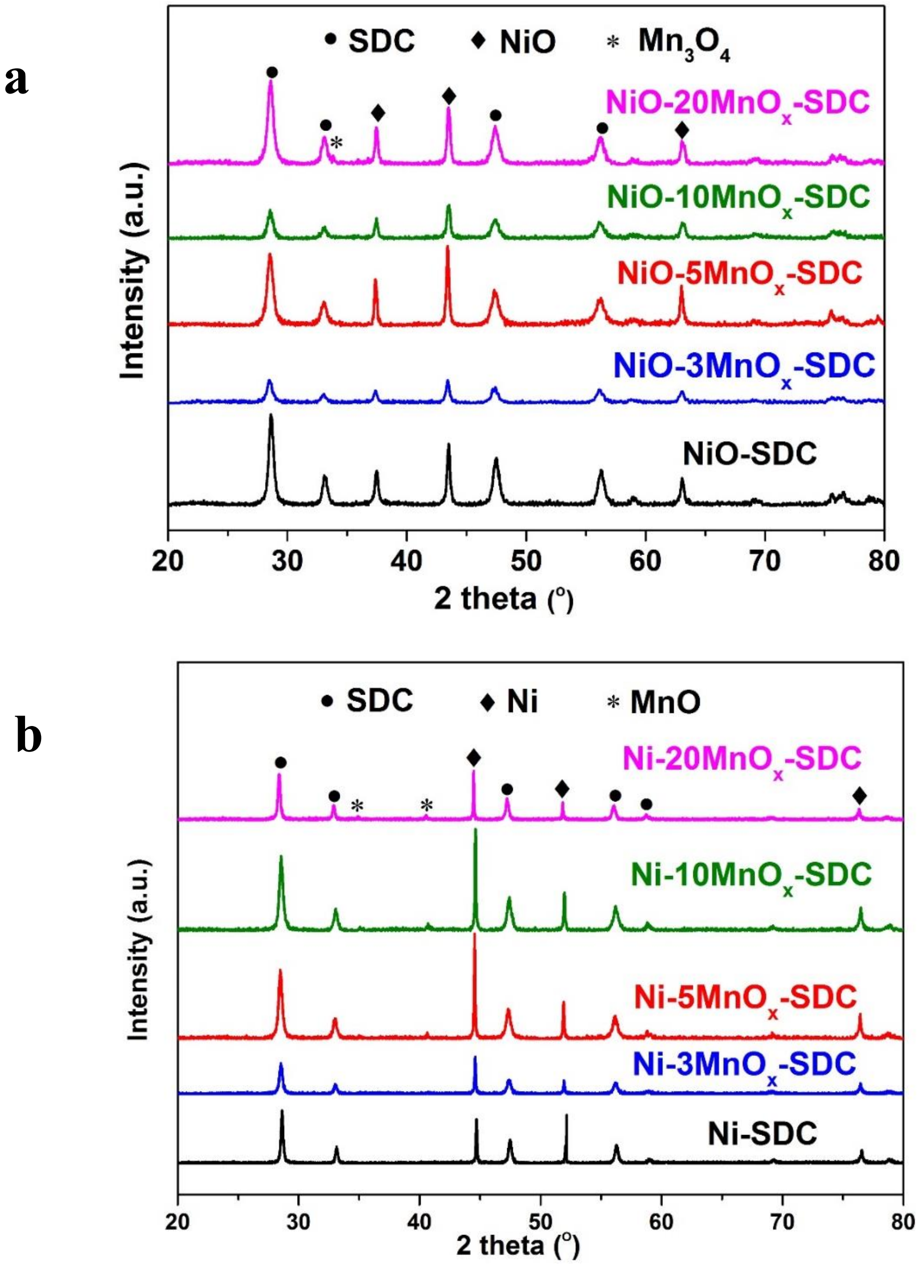

Fig. 1. XRD patterns of anode powders (a) before and (b) after reduction.

Fig. 1 presents the XRD patterns of the anode powders before and after reduction. The characteristic peaks of SDC (JCPDS #75-0158) and NiO (JCPDS #47-1049) are observed in the patterns of unreduced samples (Fig. 1a). No peak corresponding to Mn species is observed when the content of Mn is less than 0.1. When the Mn content increases to 0.2, a characteristic peak at 2θ of 34.1° appears, which is assigned to Mn_3O_4 phase (JCPDS #04-0732). No noticeable shift of SDC and NiO peaks is observed with the increase of the content of Mn, implying that Mn does not go into the lattices of SDC and NiO. After the anode powders were reduced in H_2 at 700 °C for 2 h, the peaks of NiO and Mn_3O_4 disappear, and the characteristic peaks of Ni (JCPDS#04-0850) and MnO (JCPDS #07-0230) appear instead. No shift of Ni peaks is observed with the addition of Mn species.

Fig. 2 exhibits the TPR results of anodes with different Mn contents. Two reduction peaks are observed in the result of NiO-SDC. The first peak at 349 °C is attributed to the reduction of bulk NiO [25, 26], while the second smaller peak in the range of 400-500 °C is ascribed to the reduction of NiO with a lower reducibility. With the increase of Mn content, the temperature of the first peak rises slightly, and the intensity of that peak decreases gradually. Meanwhile, the intensity of the second peak increases, indicating that the presence of manganese oxides lowers the reducibility of NiO [27]. It should be mentioned that the reduction of Mn_3O_4 to MnO also happens in the temperature range of 400-450 °C, which is involved in the second peak [28, 29]. The peak at about 300 °C could be attributed to the reduction of MnO_x (MnO_2/Mn_2O_3) to Mn_3O_4 [30-32], which becomes noticeable when the ratio of Mn to Ni is higher than 0.1:0.9.

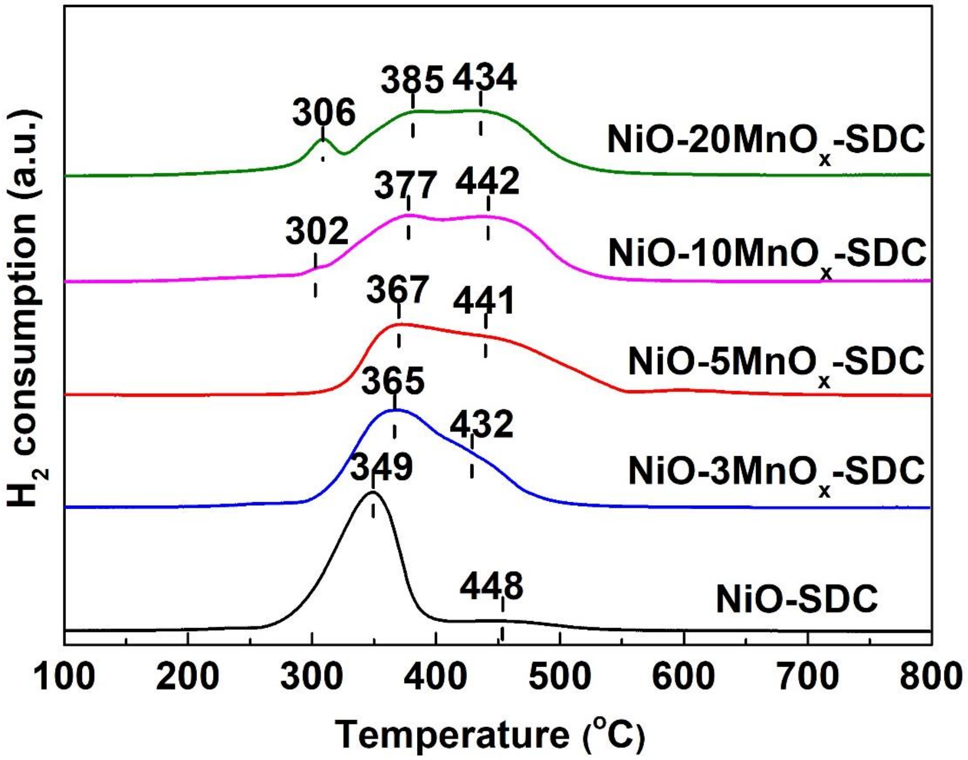

Fig. 2. H_2-TPR profiles of the anode powders with various Mn contents.

Three deconvoluted peaks are observed in the O-1s spectrum in the XPS result of Ni-SDC (Fig. 3a). The peaks at 529.1, 531.6 and 533.4 eV are ascribed to the lattice oxygen, the surface adsorbed oxygen and the oxygen in adsorbed OH groups or molecular water, respectively [32-34]. With the increase of the amount of Mn species, the content of the lattice oxygen increases, while that of the surface adsorbed oxygen decreases, as listed in Table 1. The Ni-2p$_{3/2}$ peak shifts to a higher binding energy gradually with the increase of Mn content (Fig. 3b), indicating a rise of the average valence state of Ni in the anode. That is probably due to the transfer of electrons from Ni to Mn species, which explains the decrease of the reducibility of NiO with the presence of Mn oxides, as shown in Fig. 2 [35, 36]. Meanwhile, the Mn-2p peaks shift to a lower binding energy with the increase of the content of Mn (Fig. 3c), indicating the receiving of electrons.

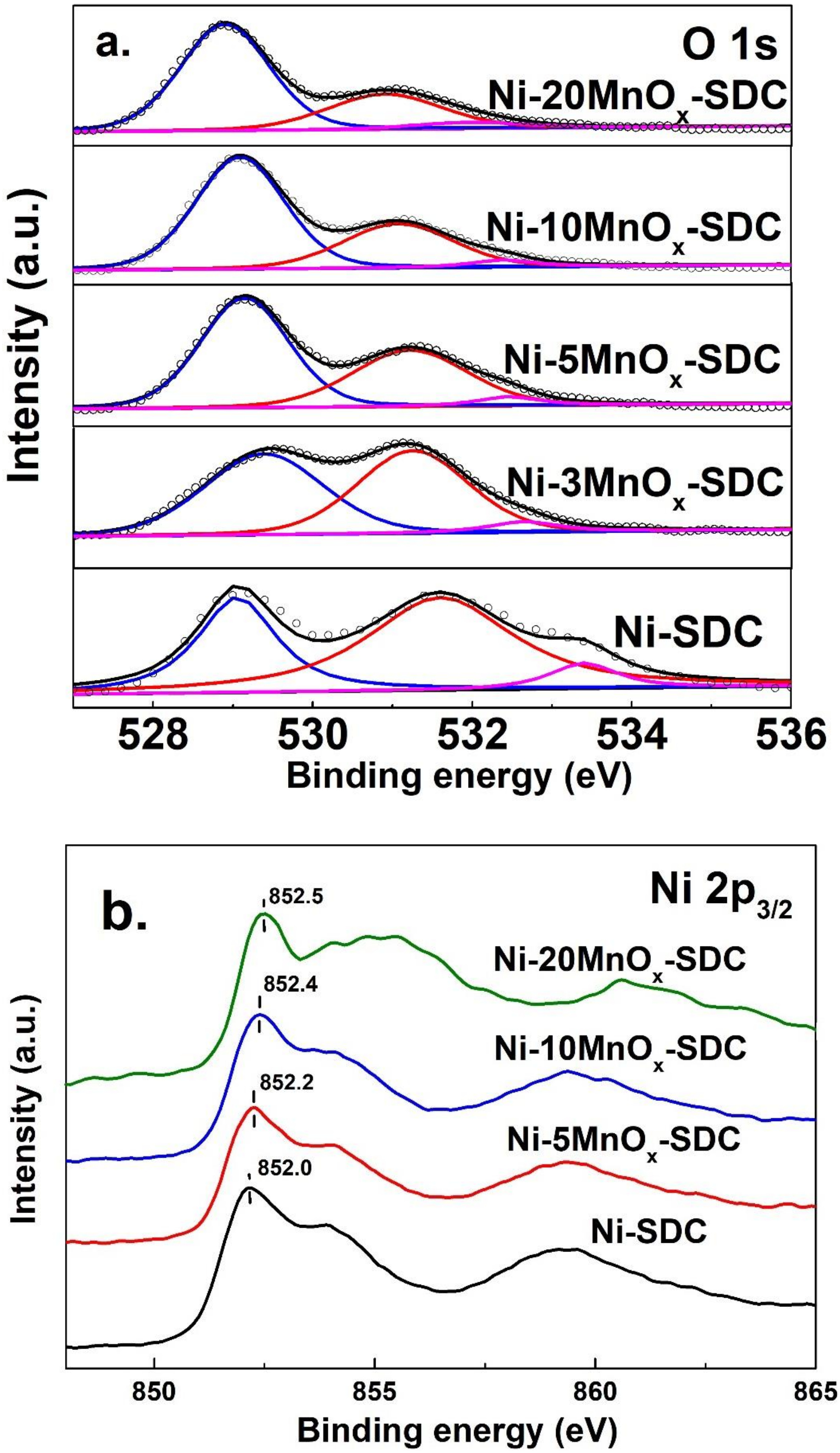
a.
O 1s
Ni-20MnO$_x$-SDC
Ni-10MnO$_x$-SDC
Ni-5MnO$_x$-SDC
Ni-3MnO$_x$-SDC
Ni-SDC
Intensity (a.u.)
528
530
532
534
536
Binding energy (eV)
b.
Ni 2p$_{3/2}$
852.5
852.4
852.2
852.0
Ni-20MnO$_x$-SDC
Ni-10MnO$_x$-SDC
Ni-5MnO$_x$-SDC
Ni-SDC
Intensity (a.u.)
850
855
860
865
Binding energy (eV)

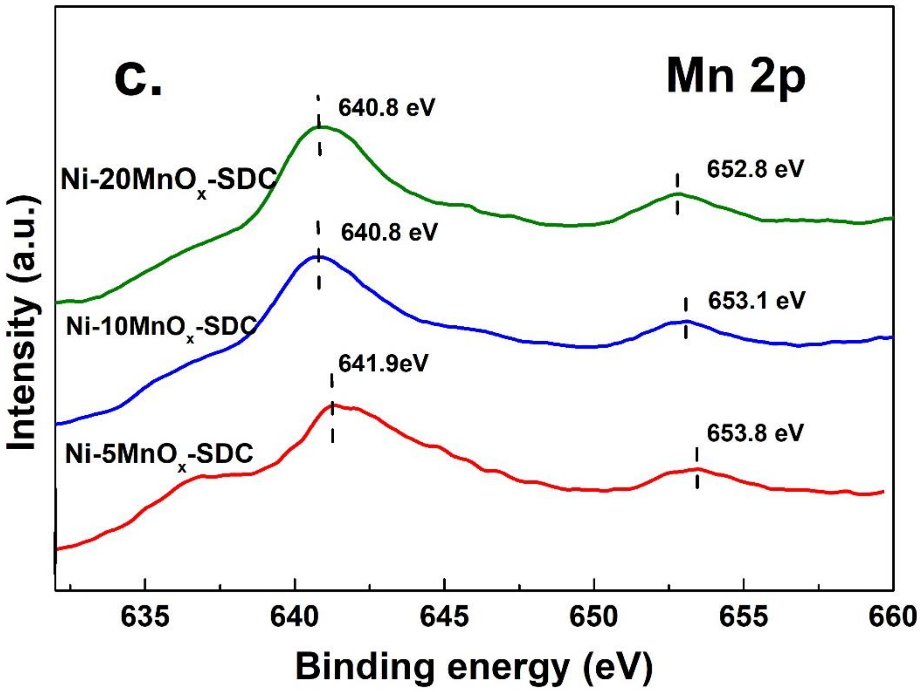

Fig. 3. (a) O-1s (b) Ni-2p$_{3/2}$ and (c) Mn-2p spectra of various anode powders after reduction.

Table 1 Amount of each surface oxygen species

Samples	Lattice oxygen		Adsorbed oxygen		Adsorbed hydroxyl and water	
	Binging Energy (eV)	Content (%)	Binging Energy (eV)	Content (%)	Binging Energy (eV)	Content (%)
Ni-SDC	529.1	32.9	531.5	59.4	533.4	7.7
Ni-3MnO-SDC	529.3	48.6	531.2	46.4	532.6	4.9
Ni-5MnO-SDC	529.2	57.1	531.2	38.4	532.5	4.4
Ni-10MnO-SDC	529.1	66.3	531.1	28.5	532.4	5.2
Ni-20MnO-SDC	528.9	70.1	530.9	23.6	532.0	6.3

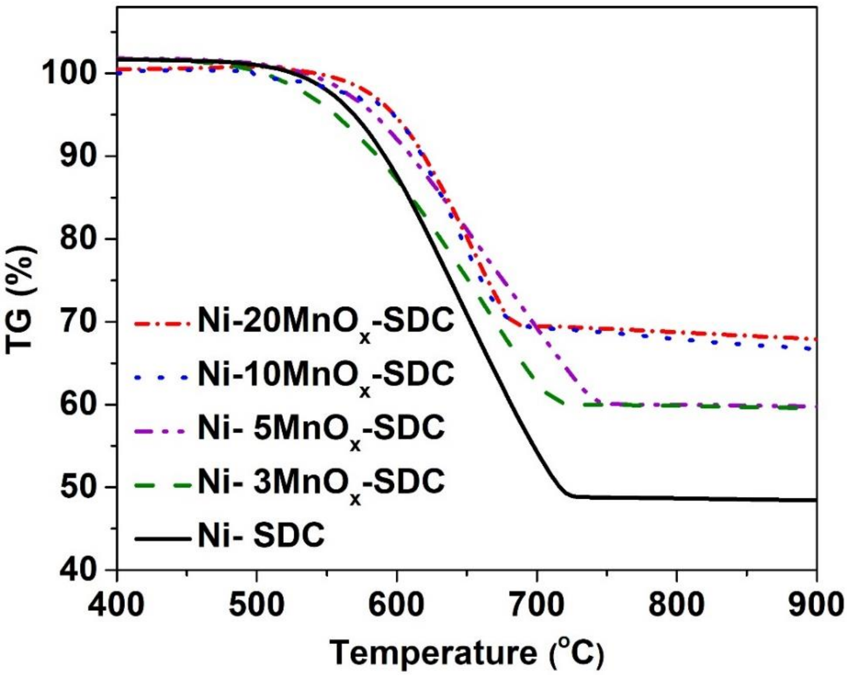

Fig. 4. TGA results of anodes with different Mn contents after carbon deposition.

Fig. 4 presents the TGA curves of various anode powders after carbon deposition. The weight loss begins at around 570 ºC is due to the oxidation of the deposited carbon. The weight loss of Ni-SDC anode reaches 49% at 900 ºC. The amount of carbon deposited generally decreases with the increase of Mn content in the anode, demonstrating that the addition of Mn oxides effectively enhance the coking resistance of the Ni-SDC anode.

3.2 The microstructure of the single cell

Fig. 5a shows the surface morphology of the NiO-5MnO$_x$-SDC anode layer. The particle size is in the range of 2-8 μm. The porous structure of the anode layer provides diffusion channels for the reactant gas. Fig. 5b presents the cross-sectional morphology of the anode-electrolyte interface of the single cell. The anode layer with a thickness of approximately 35 μm adheres closely to the electrolyte layer. The EDX mapping result of the surface of the anode demonstrates the uniform distribution of Ni, Mn and Ce in the anode layer (Fig. 5c).

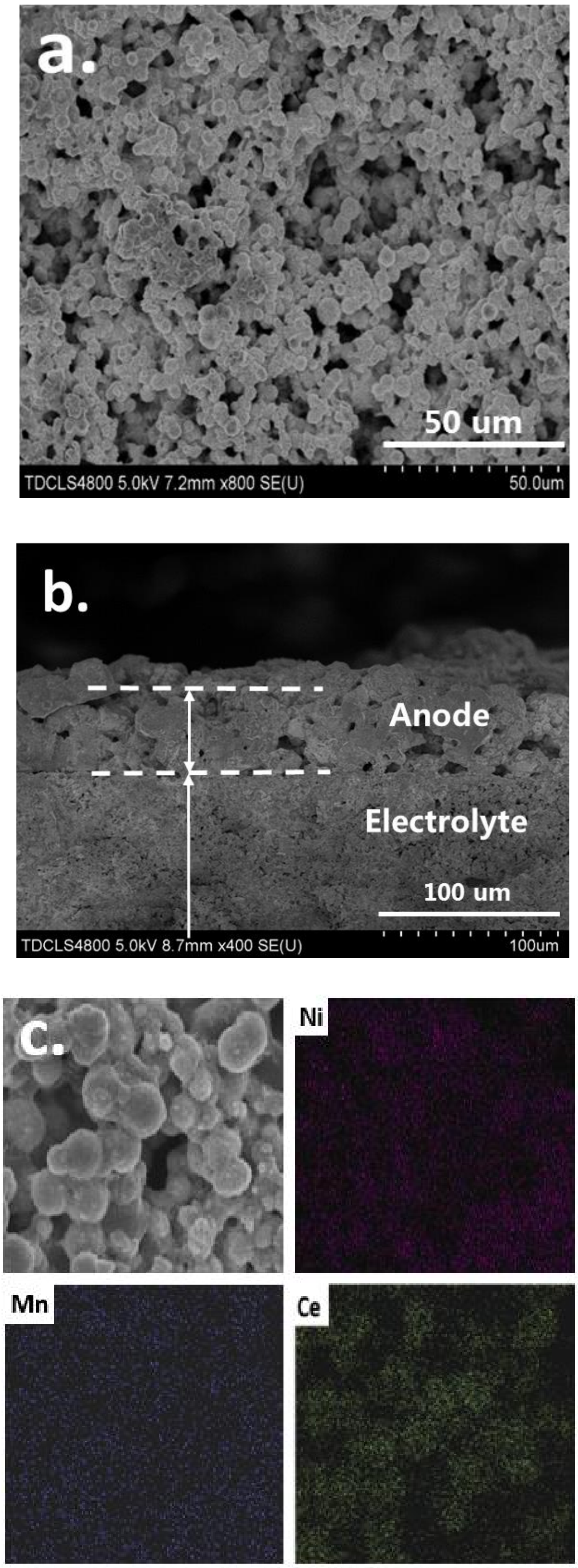

Fig. 5. SEM images of the cell with Ni-5MnO_x-SDC anode before the cell test. (a) anode surface; (b) cross-section of anode-electrolyte interface and (c) EDX element mapping of Ni, Mn and Ce.

3.3. Single cell performance

Fig. 6a illustrates the *I-V* and *I-P* curves of the cells with different anodes at 700 °C. The open circuit voltages (OCVs) of the cells are in the range of 1.05-1.10 V, close to the theoretical value. The cell with Ni-SDC anode exhibits a maximum power density ($P_{\max}$) of 433 mW cm^{-2}. The initial increase of the amount of Mn in the anode brings a remarkable rise of the $P_{\max}$. The cell with Ni-5MnO$_x$-SDC reaches the highest $P_{\max}$ of 722 mW cm^{-2}. However, the further increase of the Mn content in the anode leads to a decrease of the $P_{\max}$.

Fig. 6b shows the EIS results of the cells at 700 °C. The high-frequency intercept on the real axis and the arc are corresponding to the ohmic and the polarization resistances of the cell, respectively. The ohmic resistances of all the cells are similar, in the range of 0.26-0.29 Ω cm^2, while the electrode polarization is highly affected by the amount of Mn species in the anode. With the increase of Mn content from 0 to 0.05, the polarization resistance decreases significantly, indicating an improvement of the catalytic activity of the anode since the cathode is identical in all the cells. That could be partially attributed to the transfer of electrons from Ni to Mn species (Fig. 3b). After the donation of electrons, the 3d orbit of Ni could catch the electrons from CH_3OH more easily, facilitating the adsorption of CH_3OH on the anode surface. Meanwhile, the increase of the content of the lattice oxygen in the anode (Table 1), which plays an important role in enhancing the C-H activation during the electrochemical oxidation of methanol [37], is another probable reason for the higher catalytic activity. The further increase of the Mn content results in a decreased number of the Ni active sites, leading to an increase of the anode polarization resistance.

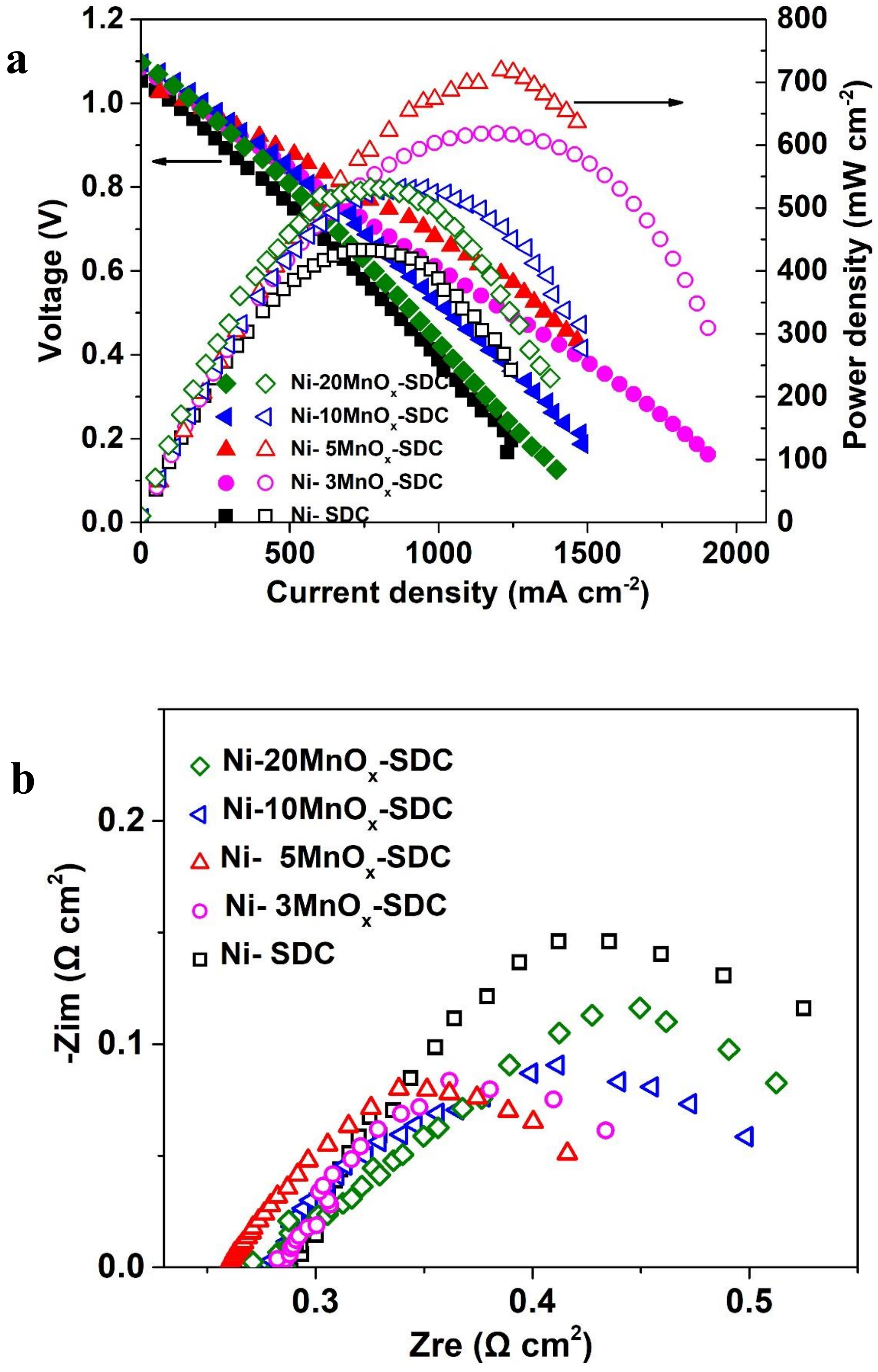

Fig. 6. (a) *I-V* and *I-P* curves and (b) impedance spectra of the fuel cells with various anodes at 700 °C with methanol as fuel.

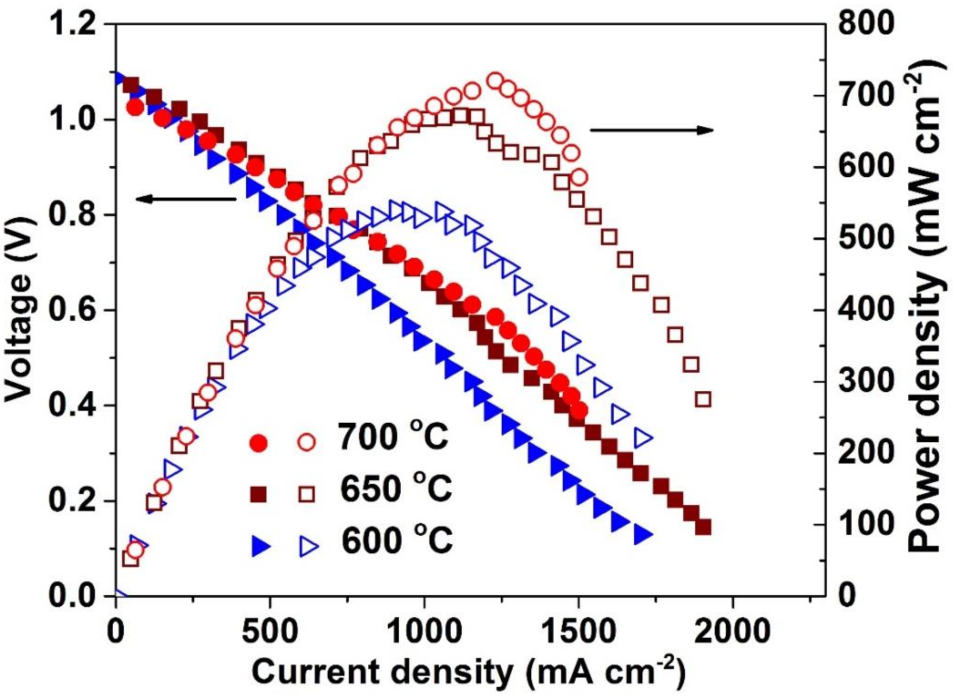

Fig. 7. *I-V* and *I-P* curves of the cell with the Ni-5MnO$_x$-SDC anode at different operating temperatures.

Fig. 7 exhibits *I-V* and *I-P* curves of the single cell with the Ni-5MnO$_x$-SDC anode in the temperature range of 600-700 ºC. The OCV is around 1.10 V. The performance of the cell increases with the rise of the temperature. The P_{max} reaches 542, 687 and 722 mW cm^{-2} at 600, 650 and 700 °C, respectively.

Fig. 8 exhibits the output voltage of the single cells with various anodes as a function of time under a current density of 200 mA cm^{-2} at 700 ºC. The voltage of the cell with the Ni-SDC anode remains stable at about 0.86 V during the first 200 min, and then drops gradually to 0.74 V within the next 120 min, which is consistent with the results in our previous work [38]. The presence of MnO$_x$ in the anode leads to a higher stability of the cell. The cells with 3% and 5% Mn in the anodes exhibit stable periods of 300 and 350 min, respectively. The cells with Ni-10MnO$_x$-SDC and Ni-20MnO$_x$-SDC anodes show a stable performance during the 480-min discharge period.

The improvement of the cell stability with the increase of the Mn content in the anode is mainly attributed to the enhanced resistance to carbon deposition, as demonstrated in Fig. 4. The increased lattice oxygen content in the anode (Table 1) could facilitate the removal of carbon deposited [31, 37, 39-41]. Meanwhile, in order to study the effect of Mn oxides on the carbon deposition process, the valence state of Mn on the surface of the Ni-10MnO_x-SDC anode after being tested under 200 mA cm^{-2} for 4 h is studied by XPS, as shown in Fig. 9. The XPS result of the anode after being exposed to methanol for 4 h under OCV is also provided for comparison. It has been proved that the split of the binding energy (ΔE) in Mn-3s spectrum strongly depends on the oxidation state of Mn [30]. The ΔE of the anode after discharge (5.6 eV) is lower than that of the anode tested under OCV (6.3 eV), indicating that the average oxidation state of Mn in the anode after discharge is higher [42, 43]. That is probably due to the partial oxidation of Mn species in a lower oxidation state, such as MnO, to a higher oxidation state, such as Mn_3O_4, by the oxygen ions from electrolyte during discharge. The formed Mn_3O_4 could be reduced by the deposited carbon to MnO subsequently [29]. The redox cycle of the Mn species in the anode during discharge is illustrated in Fig. 10. That provides another approach for the removal of the deposited carbon and leads to a higher stability of the single cell.

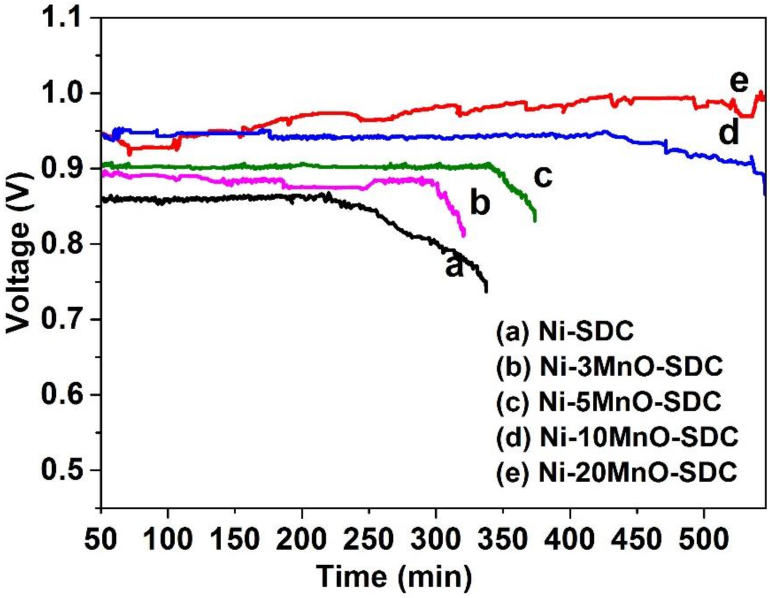

Fig. 8. Stability of the single cells under 200 mA cm^{-2} discharge at 700 °C.

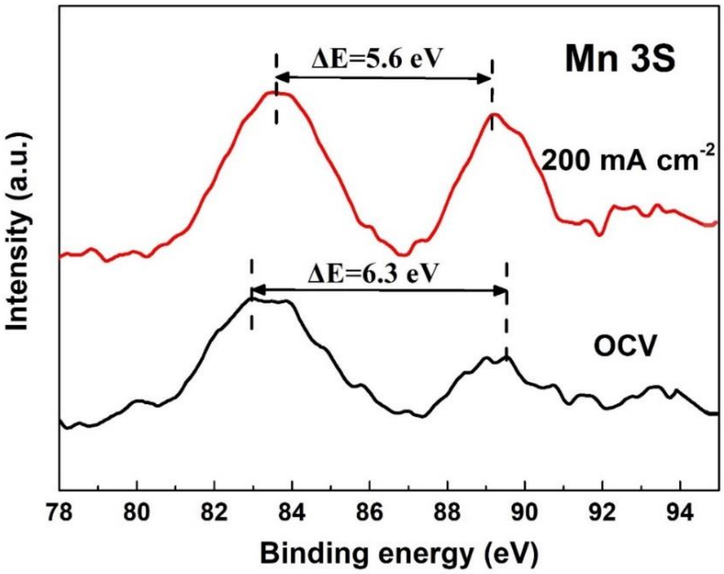

Fig. 9. Mn-3s core-level spectra of the Ni-10MnO$_x$-SDC anode after the tests under OCV and 200 mA cm^{-2} discharge for 4 h.

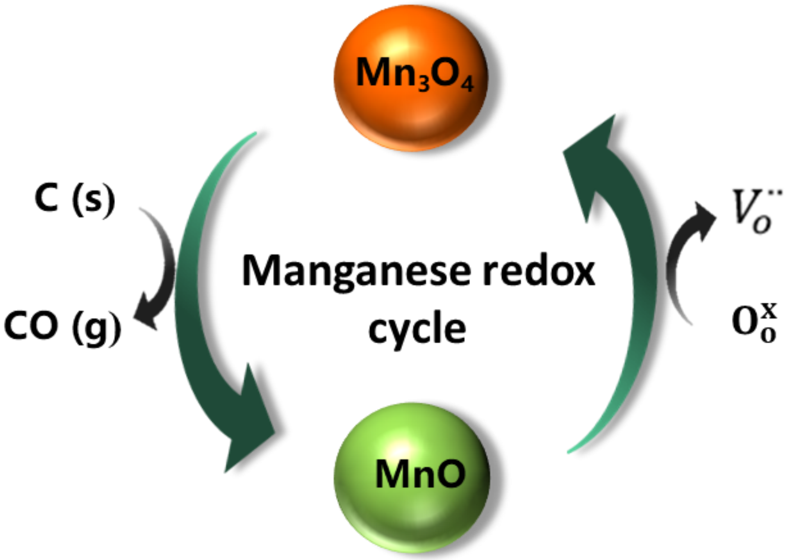

Fig.10. Schematic of the carbon removal process based on the redox cycle of the Mn species in the anode during discharge.

4. Conclusions

Ni-MnO$_x$-SDC composites are studied as anode materials for SOFCs with methanol as the fuel. The presence of Mn in the anode leads to a high content of the lattice oxygen and the transfer of electrons from Ni to Mn species, both of which increase the catalytic activity of the anode for the electrochemical oxidation of methanol. The single cell with Ni-5MnO$_x$-SDC anode and SDC-carbonate composite electrolyte exhibits the highest $P_{\max}$ of 722 mW cm^{-2} at 700 °C. The further increase of the Mn content results in a lower cell performance probably due to the decrease of the number of Ni active sites. The increase of the lattice oxygen content facilitates the removal of carbon deposited on the anode. Meanwhile, the redox cycle of the Mn species is also a potential way for the oxidation of the carbon, leading to a higher stability of the cell. The single cells with Ni-10MnO$_x$-SDC and Ni-20MnO$_x$-SDC anodes exhibit stable outputs during the 480-min discharge.

Acknowledgments

The financial support of NSF of China under contract numbers 51402210 and 21120102039, the support of Tianjin Municipal Science and Technology Commission under contract numbers 15JCQNJC06500, and the support of the Ministry of Education of China under contract number 20130032120023 are gratefully acknowledged. The work has been also supported by the Program of Introducing Talents to the University Disciplines under file number B06006, and the Program for Changjiang Scholars and Innovative Research Teams in Universities under file number IRT 0641.

References

[1] W. Wang, H. Zhu, G. Yang, H.J. Park, D.W. Jung, C. Kwak, Z. Shao, J. Power Sources, 258 (2014) 134-141.
[2] T. Hibino, A. Hashimoto, T. Inoue, J. Tokuno, S. Yoshida, M. Sano, Science, 288 (2000) 2031.
[3] E. Nikolla, A. Holewinski, J. Schwank, S. Linic, J. Am. Chem. Soc., 128 (2006) 11354.
[4] C. Su, Y. Wu, W. Wang, Y. Zheng, R. Ran, Z. Shao, J. Power Sources, 195 (2010) 1333-1343.
[5] W. Wang, R. Ran, Z. Shao, J. Power Sources, 196 (2011) 90-97.
[6] J. Qu, W. Wang, Y. Chen, X. Deng, Z. Shao, Appl. Energy, 164 (2016) 563-571.

[7] G.A. Olah, Angew. Chem. Int. Ed. Engl., 44 (2005) 2636-2639.
[8] M. Cimenti, J.M. Hill, J. Power Sources, 195 (2010) 54-61.
[9] H. Li, Y. Tian, Z. Wang, F. Qie, Y. Li, RSC Advances, 2 (2012) 3857.
[10] R. Thattarathody, M. Sheintuch, Appl. Catal. A: Gen, 540 (2017) 47-56.
[11] S. Alayoglu, K. An, G. Melaet, S. Chen, F. Bernardi, L.W. Wang, A.E. Lindeman, N. Musselwhite, J. Guo, Z. Liu, M.A. Marcus, G.A. Somorjai, J. Phys. Chem. C, 117 (2013) 26608-26616.
[12] A. Fuerte, R.X. Valenzuela, M.J. Escudero, L. Daza, J. Power Sources, 196 (2011) 4324-4331.
[13] H. Kan, H. Lee, Appl. Catal., B: Environ., 97 (2010) 108-114.
[14] K. Cheng, H. Chen, W. Weng, C. Song, P. Du, G. Shen, G. Han, J. Alloys Compd., 541 (2012) 65-69.
[15] Y. Ma, X. Wang, R. Raza, M. Muhammed, B. Zhu, Int. J. Hydrogen Energy, 35 (2010) 2580-2585.
[16] H. Chen, A. Sayari, A. Adnot, F.Ç. Larachi, Applied Catalysis B Environmental, 32 (2001) 195-204.
[17] S.H. Seok, S.H. Han, J.S. Lee, Applied Catalysis A General, 215 (2001) 31-38.
[18] J. Zhao, X. Xu, W. Zhou, Z. Zhu, Fuel Process. Technol., 161 (2017) 241-247.
[19] L.M.P. Garcia, D.A. Macedo, G.L. Souza, F.V. Motta, C.A. Paskocimas, R.M. Nascimento, Ceram. Int., 39 (2013) 8385-8392.
[20] X. Dong, L. Tian, J. Li, Y. Zhao, Y. Tian, Y. Li, J. Power Sources, 249 (2014) 270-276.
[21] B. Zhu, L. Fan, P. Lund, Appl. Energy, 106 (2013) 163-175.
[22] L. Jia, Y. Tian, Q. Liu, C. Xia, J. Yu, Z. Wang, Y. Zhao, Y. Li, J. Power Sources, 195 (2010) 5581-5586.
[23] J. Yu, B. Yu, Y. Li, Int. J. Hydrogen Energy, 38 (2013) 16615-16622.
[24] G. Ding, T. Gan, J. Yu, P. Li, X. Yao, N. Hou, L. Fan, Y. Zhao, Y. Li, Catal. Today, 298 (2017) 250-257.
[25] M. Peymani, S.M. Alavi, M. Rezaei, Int. J. Hydrogen Energy, 41 (2016) 6316-6325.
[26] J. Marrero-Jerez, E. Chinarro, B. Moreno, M.T. Colomer, J.R. Jurado, P. Núñez, Ceram. Int., 40 (2014) 3469-3475.
[27] H. Zhao, K. Fang, J. Zhou, M. Lin, Y. Sun, Int. J. Hydrogen Energy, 41 (2016) 8819-8828.
[28] E. Poggio-Fraccari, J. Sambeth, G. Baronetti, F. Mariño, Int. J. Hydrogen Energy, 39 (2014) 8675-8681.
[29] F. Touahra, M. Sehailia, D. Halliche, K. Bachari, A. Saadi, O. Cherifi, Int. J. Hydrogen Energy, 41 (2016) 21140-21156.
[30] J. Trawczyński, B. Bielak, W. Miśta, Appl. Catal., B: Environ., 55 (2005) 277-285.
[31] W. Tang, J. Li, X. Wu, Y. Chen, Catal. Today, 258 (2015) 148-155.
[32] W. Tang, Y. Deng, W. Li, J. Li, G. Liu, S. Li, X. Wu, Y. Chen, Catal. Sci. Technol., 6 (2016) 1710-1718.
[33] K. Jirátová, J. Mikulová, J. Klempa, T. Grygar, Z. Bastl, F. Kovanda, Appl. Catal. A: Gen, 361 (2009) 106-116.
[34] L. Yu, G. Diao, F. Ye, M. Sun, J. Zhou, Y. Li, Y. Liu, Catal. Lett., 141 (2010) 111-119.
[35] L. Zhao, Y. Wei, Y. Huang, Y. Liu, Catal. Today, 259 (2016) 430-437.
[36] Z. Bian, X. Meng, M. Tao, Y. Lv, Z. Xin, Fuel, 179 (2016) 193-201.
[37] M.D. Salazar-Villalpando, B. Reyes, Int. J. Hydrogen Energy, 34 (2009) 9723-9729.

[38] P. Li, B. Yu, J. Li, X. Yao, Y. Zhao, Y. Li, J. Power Sources, 320 (2016) 251-256.
[39] R. Ran, X. Wu, D. Weng, J. Fan, J. Alloys Compd., 577 (2013) 288-294.
[40] H. Song, U. Ozkan, J. Catal., 261 (2009) 66-74.
[41] K. Sutthiumporn, S. Kawi, Int. J. Hydrogen Energy, 36 (2011) 14435-14446.
[42] Z. Gao, Z. Mao, C. Wang, Z. Liu, Int. J. Hydrogen Energy, 35 (2010) 12897-12904.
[43] M. Liu, S. Wang, T. Chen, C. Yuan, Y. Zhou, S. Wang, J. Huang, J. Power Sources, 274 (2015) 730-735.